2012-01

Coordination Polymers Based on [Cp*FeACHTUNGTRENUNG(h5-P5)]: MAS NMR Studies

Chemistry - A European Journal,Weinheim : Wiley-VCH Verlag,v. 18, n. 4, p. 1168-1179, Jan. 2012
http://www.producao.usp.br/handle/BDPI/49505

CHEMISTRY
A EUROPEAN JOURNAL

DOI: 10.1002/chem.201102107

Coordination Polymers Based on [Cp*Fe(η^5-P_5)]: Solid-State Structure and MAS NMR Studies

Fabian Dielmann,[a] Andrea Schindler,[a] Sabine Scheuermayer,[a] Junfeng Bai,[b] Roger Merkle,[a] Manfred Zabel,[a] Alexander V. Virovets,[c] Eugenia V. Peresypkina,[c] Gunther Brunklaus,[d, e] Hellmut Eckert,*[e] and Manfred Scheer*[a]

Dedicated to Professor Klaus Jurkschat on the occasion of his 60th birthday

Abstract: Slow diffusion reactions of the pentaphosphaferrocene [Cp*Fe(η^5-P_5)] (Cp* = η^5-C_5Me_5 (**1**)) with CuX (X = Cl, Br, I) in different stoichiometric ratios and solvent mixtures result in the formation of one- and two-dimensional polymeric compounds **2**–**6** with molecular formula $[\{Cu(\mu\text{-}X)\}\{Cp^*Fe(\mu_3,\eta^5\text{:}\eta^1\text{:}\eta^1\text{-}P_5)\}]_n$ (X = Cl (**2a**), I (**2′c**)), $[\{Cu(\mu\text{-}I)\}\{Cp^*Fe(\mu_3,\eta^5\text{:}\eta^1\text{:}\eta^1\text{-}P_5)\}]_n$ (**3**), $[\{CuX\}\{Cp^*Fe(\mu_4,\eta^5\text{:}\eta^1\text{:}\eta^1\text{:}\eta^1\text{-}P_5)\}]_n$ (X = Cl (**4a**), Br (**4b**), I (**4c**), Br (**4′b**), I (**4′c**)), $[\{Cu_3(\mu\text{-}I)_2(\mu_3\text{-}I)\}\{Cp^*Fe(\mu_5,\eta^5\text{:}\eta^1\text{:}\eta^1\text{:}\eta^1\text{:}\eta^1\text{-}P_5)\}]_n$ (**5**) and $[\{Cu_4(\mu\text{-}X)_4(CH_3CN)\}\{Cp^*Fe(\mu_7,\eta^5\text{:}\eta^2\text{:}\eta^1\text{:}\eta^1\text{:}\eta^1\text{:}\eta^1\text{:}\eta^1\text{-}P_5)\}]_n$ (X = Cl (**6a**), Br (**6b**)), respectively. The polymeric compounds have been characterised by single-crystal X-ray diffraction analyses and, for selected examples, by magic angle spinning (MAS) NMR spectroscopy. The solid-state structures demonstrate the versatile coordination modes of the *cyclo*-P_5 ligand of **1**, extending from two to five coordinating phosphorus atoms in either σ or σ-and-π fashion. In compounds **2a**, **2′c** and **3**, two phosphorus atoms of **1** coordinate to copper atoms in a 1,2 coordination mode (**2a**, **2′c**) and an unprecedented 1,3 coordination mode (**3**) to form one-dimensional polymers. Compounds **4a**–**c**, **4′b**, **4′c** and **5** represent two-dimensional coordination polymers. In compounds **4**, three phosphorus atoms coordinate to copper atoms in a 1,2,4 coordination mode, whereas in **5** the *cyclo*-P_5 ligand binds in an unprecedented 1,2,3,4 coordination mode. The crystal structures of **6a**,**b** display a tilted tube, in which all P atoms of the *cyclo*-P_5 ligand are coordinated to copper atoms in σ- and π-bonding modes.

Keywords: coordination polymers · MAS NMR spectroscopy · P ligands · self-assembly · solid-state structures · supramolecular chemistry

Introduction

The self-organisation of discrete units to form supramolecular aggregates and networks is a fascinating field of contemporary chemical research.[1] In contrast to other approaches in this area, we use organometallic E_n[2] and E_mS_n ligand[3] complexes (E = P, As) as connecting moieties between metal cations instead of the already well-studied N- and O-donor linkers. We have shown that very different P_n ligand complexes, such as $[\{CpM(CO)_2\}_2(\mu,\eta^2\text{:}\eta^2\text{-}P_2)]$ (M = Cr, Mo),[4] $[Cp^RMo(CO)_2(\eta^3\text{-}P_3)]$[5] and $[Cp^RFe(\eta^5\text{-}P_5)]$ (Cp^R: Cp* = η^5-C_5Me_5 (**1**), Cp^{Et} = η^5-C_5Me_4Et),[6] can be used as connecting moieties between late-transition-metal cations to form extended structures. Reactions of the former complex with copper(I) and silver(I) cations result in the formation of infinite-chain or zigzag polymeric structures.[4] However, the *cyclo*-P_5 ring of the pentaphosphaferrocene possesses multiple coordination possibilities. Thus, its reactions with Cu^I halides result in the formation of either one- or two-dimensional polymeric compounds,[6a] which show a 1,2 (type **A**) and 1,2,4 (type **D**) coordination mode. Under special reaction conditions, spherical nano-sized aggregates are formed,[7] in which all of the P atoms coordinate towards Lewis acidic Cu centres.

[a] Dr. F. Dielmann, Dr. A. Schindler, Dipl.-Chem. S. Scheuermayer, Dipl.-Chem. R. Merkle, Dr. M. Zabel, Prof. Dr. M. Scheer
Institut für Anorganische Chemie der Universität Regensburg
93040 Regensburg (Germany)
Fax: (+49) 941-943-4439
E-mail: manfred.scheer@chemie.uni-regensburg.de

[b] Prof. Dr. J. Bai
Coordination Chemistry Institute and
the State Key Laboratory of Coordination Chemistry
Nanjing University, 210093 Nanjing (P.R. China)

[c] Dr. A. V. Virovets, Dr. E. V. Peresypkina
Nikolaev Institute of Inorganic Chemistry Siberian Division of RAS
Acad. Lavrentyev prosp. 3
630090 Novosibirsk (Russia)

[d] Dr. G. Brunklaus
Max-Planck-Institut für Polymerforschung
55128 Mainz (Germany)

[e] Dr. G. Brunklaus, Prof. Dr. H. Eckert
Institut für Physikalische Chemie der
Westfälischen Wilhelms-Universität Münster
48149 Münster (Germany)
Fax: (+49) 253-83-29159
E-mail: eckerth@uni-muenster.de

Supporting information for this article is available on the WWW under http://dx.doi.org/10.1002/chem.201102107.

The crystal structures of all compounds obtained so far were readily determined by single-crystal X-ray structure analysis because suitable crystals were accessible. Problems to determine the exact nature of the formed compound may be encountered in case of rather small or twinned crystals or when possibly less-defined microcrystalline powders are obtained, though sophisticated powder X-ray diffraction techniques are available.[8] Because many of the polymeric products are insoluble in common solvents, neither solution NMR spectroscopy nor mass spectrometry are viable tools for further characterization. In contrast, solid-state NMR spectroscopy provides unique selectivity for the differentiation of chemically distinct sites on the basis of the NMR chemical shift, thereby revealing (molecular) species present in a sample, including major products, possible side products and even polymorphs. Therefore, we performed a systematic investigation by using solid-state MAS NMR spectroscopy to identify the coordination pattern of the *cyclo*-P_5 ring based on its characteristic ^{31}P NMR spectrum in the solid state.

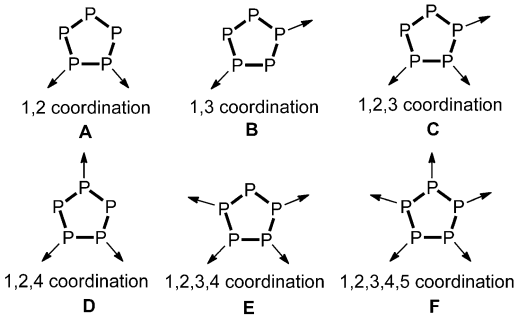

Furthermore, by varying both the solvent mixture and the stoichiometric ratios we have successfully prepared and characterised the previously unknown coordination polymers $[\{Cu(\mu\text{-}I)\}\{Cp^*Fe(\mu_3,\eta^5{:}\eta^1{:}\eta^1\text{-}P_5)\}]_n$ (**2′c**), $[\{Cu(\mu\text{-}I)\}\{Cp^*Fe(\mu_3,\eta^5{:}\eta^1{:}\eta^1\text{-}P_5)\}]_n$ (**3**), $[\{CuX\}\{Cp^*Fe(\mu_4,\eta^5{:}\eta^1{:}\eta^1{:}\eta^1\text{-}P_5)\}]_n$ (X = Br (**4′b**), I (**4′c**)), $[\{Cu_3(\mu\text{-}I)_2(\mu_3\text{-}I)\}\{Cp^*Fe(\mu_5,\eta^5{:}\eta^1{:}\eta^1{:}\eta^1{:}\eta^1\text{-}P_5)\}]_n$ (**5**) and $[\{Cu_4(\mu\text{-}X)_4(CH_3CN)\}\{Cp^*Fe(\mu_7,\eta^5{:}\eta^2{:}\eta^1{:}\eta^1{:}\eta^1{:}\eta^1{:}\eta^1\text{-}P_5)\}]_n$ (X = Cl (**6a**), Br (**6b**)), which reveal the unprecedented coordination modes **B** (in **3**), **E** (in **5**) and **F** (in **6a**,**b**) as well as the already observed coordination types **A** (in **2′c**) and **D** (in **4′b** and **4′c**). Mode F was so far only found in spherical and soluble compounds, not in polymeric structures. In addition, we discuss complementary structural information of selected new and previously reported polymeric compounds, such as $[\{Cu(\mu\text{-}Cl)\}\{Cp^*Fe(\mu_3,\eta^5{:}\eta^1{:}\eta^1\text{-}P_5)\}]_n$ (**2a**),[6a] $[\{CuX\}\{Cp^*Fe(\mu_4,\eta^5{:}\eta^1{:}\eta^1{:}\eta^1\text{-}P_5)\}]_n$ (X = Cl (**4a**),[7a] Br (**4b**), I (**4c**)[6a]) and $[Ag\{Cp^*Fe(\eta^5{:}\eta^2{:}\eta^1\text{-}P_5)\}_2]_n[Al\{OC(CF_3)_3\}_4]_n$ (**7**),[6b] respectively, as derived from detailed solid-state MAS NMR spectroscopy investigations.

Results and Discussion

Synthesis of the products: Compounds **2–6** are formed by diffusion reactions of **1** with CuX (X = Cl, Br, I) at room temperature depending on the composition of the solvent mixture (dichloromethane, benzene, toluene or *ortho*-dichlorobenzene combined with acetonitrile) and stoichiometric ratio of the reactants (Scheme 1). Interestingly, compounds **2a**·0.5*n*C_6H_6 and **4′b** were obtained by using Cu^{II} halogenides rather than Cu^I salts, which reveals that a reduction occurs, probably combined with an oxidation of the pentaphosphaferrocene **1**. However, no spectroscopic evidence of oxidised P-containing products could be found. A similar effect was earlier found by using $[\{CpMo(CO)_2\}_2(\mu,\eta^2{:}\eta^2\text{-}P_2)]$ in the reaction with CuX_2 (X = Cl, Br, I).[4d] The isolated crystalline compounds are stable under nitrogen and insoluble in common solvents. Thus, products **2–6** were characterized by single-crystal X-ray diffraction analyses and for selected compounds by solid-state ^{31}P NMR spectroscopy. It should be noted that compounds marked with a prime (′) reveal a different packing mode of their 1D or 2D strands in the solid state upon inclusion of solvent molecules in the crystal lattice.

X-ray crystallographic characterization: The X-ray structure analyses of compounds **2a**·0.5*n*CH_2Cl_2[6a] as well as **4a**[7a] **4b** and **4c**[6a] have already been reported by us. The new compounds **2a**·0.5*n*C_6H_6, **2′c**, **3**, **4′b**, **4′c**, **5** and **6a**,**b** have been characterized by single crystal X-ray diffraction and the crystallographic details are summarized in Tables 1 and 2.

The coordination of the pentaphosphaferrocene $[Cp^*Fe(\eta^5\text{-}P_5)]$ (**1**) to Cu^I halides generally has only marginal influences on the bond parameters of the starting material.[6b,9] Similarly, a slight shortening of the P–P bond lengths is induced by σ coordination of the *cyclo*-P_5 ligand to the copper atoms in coordination polymers **2′c**, **3**, **4′b**, **4′c** and **5**. However, additional π coordination of the *cyclo*-P_5 ligand to copper centres in **6a**,**b** results in a small elongation of the respective P–P bond lengths compared to the uncoordinated complex $[Cp^*Fe(\eta^5\text{-}P_5)]$ (**1**; av 2.117(4) Å).[6b,9]

*Crystal structure of **2′c***: Compound **2′c**, the first 1D polymer of **1** containing CuI moieties, crystallizes as brown-black needles in the orthorhombic space group $Pna2_1$. A section of the 1D polymeric structure of **2′c** is depicted in Figure 1. The infinite chain structure consists of Cu_2I_2 four-membered rings, which are coordinated by pentaphosphaferrocene molecules **1**. The 1,2 coordination of the *cyclo*-P_5 ligands to the Cu centres lead to a structural motif of alternating Cu_2I_2 four-membered and Cu_2P_4 six-membered rings, which are tilted by 75.67(2)° towards each other. In compound **2′c**, complexes **1** have the same orientation on each side of the plane spanned by the Cu_2I_2 rings, whereas in polymer **2a** complexes **1** are oriented alternately. Nevertheless, in the crystal lattice of both polymers **2a** and **2′c**, complexes **1** stack with intermolecular Cp*···P_5 contacts around 3.5 Å.[10]

*Crystal structure of **3***: Brown compound **3** crystallises in the acentric tetragonal space group $P4_12_12$. A section of the 1D polymeric structure of **3** is shown in Figure 2. Cu_2I_2 four-membered rings are connected by the pentaphosphaferro-

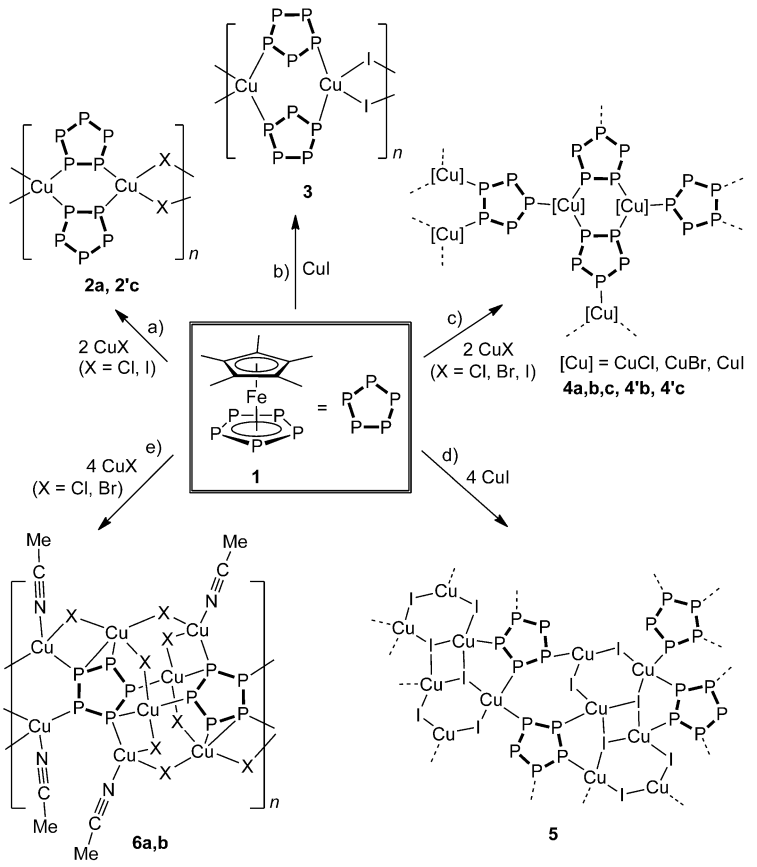

Scheme 1. The syntheses of **2–6** were carried out by diffusion experiments at RT. a) CuCl/[Cp*Fe(η^5-P_5)] 1:1, CH_2Cl_2/CH_3CN[6a] or benzene/CH_3CN (**2a**, in the latter case $CuCl_2$ was used); CuI/[Cp*Fe(η^5-P_5)] 2:1, THF/CH_3CN (**2′c**); b) CuI/[Cp*Fe(η^5-P_5)] 2:1, *o*-dichlorobenzene/CH_3CN in the presence of [$CoCp_2$]; c) CuCl/[Cp*Fe(η^5-P_5)] 2:1, toluene/CH_3CN (**4a**); CuX/[Cp*Fe(η^5-P_5)] 1:1 (X = Br, I), CH_2Cl_2/CH_3CN (**4b**,**c**); CuX/[Cp*Fe(η^5-P_5)] 1:1 (X = Br, I), benzene/CH_3CN (**4′b**,**c**; for **4′b** $CuBr_2$ was used); d) CuI/[Cp*Fe(η^5-P_5)] 4:1, *o*-dichlorobenzene/CH_3CN (**5**); e) CuX/[Cp*Fe(η^5-P_5)] 4:1 (X = Cl, Br), *o*-dichlorobenzene/CH_3CN (**6a**,**b**).

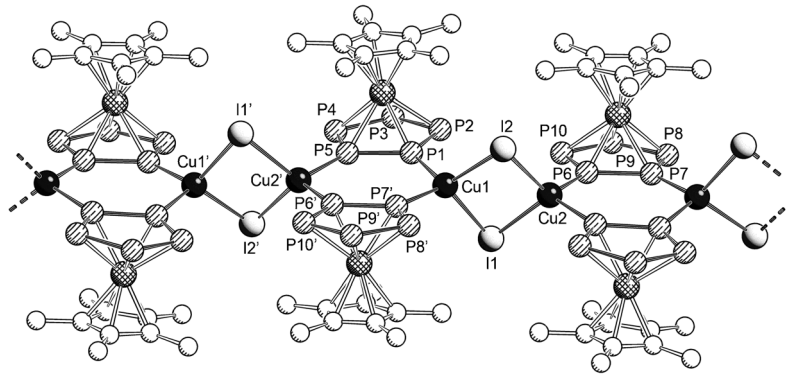

Figure 1. Section of the 1D polymeric structure of **2′c**. Hydrogen atoms are omitted for clarity. Selected bond lengths [Å]: P1–P2 2.103(2), P1–P5 2.1150(19), P2–P3 2.116(2), P3–P4 2.109(2), P4–P5 2.1079(19), P6–P7 2.1168(19), P6–P10 2.111(2), P7–P8 2.1066(19), P8–P9 2.117(2), P9–P10 2.113(2), Cu1–P1 2.2913(15), Cu1–P7′ 2.2756(15), Cu2–P6 2.2923(16), Cu2–P5 2.2865(16), Cu1–I1 2.6481(8), Cu1–I2 2.6295(8), Cu2–I1 2.6425(8), Cu2–I2 2.6525(8).

cene molecules in an unprecedented 1,3 coordination mode in contrast to compounds **2**, which displays a 1,2 linking mode. In this way, 12-membered $Cu_4I_2P_6$ rings are formed. The Cu_2I_2 rings are essentially planar and parallel to each other. In **3**, the opposing complexes **1** have reverse orientation, whereas the neighbouring complexes are twisted by 65.05(8)°. Remarkably, the 1D polymeric chains of **3** in the crystal lattice are separated by *ortho*-dichlorobenzene molecules each stacking between two Cp* ligands of neighbouring strands.[10]

*Crystal structure of **4′b** and **4′c***: Compounds **4′b** and **4′c** crystallize as brown plates in the tetragonal space group $P\bar{4}2_1c$. A section of the 2D polymeric crystal structure is depicted in Figure 3. The *cyclo*-P_5 ligands of the pentaphosphaferrocene complexes **1** are connected by Cu^I ions in a 1,2,4 coordination mode. This leads to an undulating 2D sheet structure with alternating Cu_2P_4 six-membered rings and Cu_4P_{12} cycles, which is isostuctural to **4a–c**. However, in contrast to the parallel arrangement of the layers in compounds **4a–c**, the orientation of the layers in **4′b** and **4′c** induce the formation of voids just big enough to host a benzene molecule (Figure 4).[10]

*Crystal structure of **5***: Compound **5** crystallizes as orange plates in the monoclinic space group $P2_1/c$. The X-ray structure analysis reveals a 2D polymeric structure (Figure 5), which consists of pentaphosphaferrocene molecules **1** linked by Cu_6I_6 units. Each bridging Cu_6I_6 unit contains an inversion centre and consists of two six-membered Cu_3I_3 rings, which are connected by two comparably long Cu–I bonds (2.832(3) Å) to form a central four-membered Cu_2I_2 ring. The *cyclo*-P_5 ligands of complexes **1** coordinate to the Cu_6I_6 units through four of their five P atoms. The resulting 1,2,3,4 coordination mode is unprecedented among pentaphosphaferrocene coordination polymers, and facilitates the formation of a 2D sheet structure in which single layers are separated by

Table 1. Crystallographic data of compounds **2a**, **2′c**, **3** and **4′b**.

	2a·0.5*n* C_6H_6	**2′c**·0.5*n* THF	**3**·0.5*n* $C_6H_4Cl_2$	**4′b**·0.25*n* C_6H_6
formula	$C_{26}H_{36}Cl_2Cu_2Fe_2P_{10}$	$C_{24}H_{38}Cu_2OFe_2I_2P_{10}$	$C_{26}H_{34}Cl_2Cu_2Fe_2I_2P_{10}$	$C_{11.5}H_{16.5}BrCuFeP_5$
M_r	967.95	1144.85	1219.71	508.90
crystal size [mm]	0.46×0.31×0.16	0.24×0.09×0.03	0.27×0.02×0.01	0.54×0.43×0.16
T [K]	123(1)	150(2)	94(2)	123(1)
space group	orthorhombic	orthorhombic	tetragonal	tetragonal
crystal system	*Pnma*	$Pna2_1$	$P4_12_12$	$P\bar{4}2_1c$
a [Å]	13.7365(3)	13.8066(1)	16.4846(2)	11.9920(2)
b [Å]	31.0655(8)	16.7490(2)	16.4846(2)	11.9920(2)
c [Å]	17.2262(4)	16.4418(1)	29.1575(7)	23.9465(6)
α [°]	90	90	90	90
β [°]	90	90	90	90
γ [°]	90	90	90	90
V [Å^3]	7351.0(3)	3802.11(6)	7923.3(2)	3443.70(12)
Z	8	4	8	8
ρ_{calcd} [g cm^{-3}]	1.749	2.000	2.045	1.963
μ [mm^{-1}]	2.516	24.158	24.432	4.847
Θ range [°]	2.70–29.16	3.77–63.02	3.08–66.73	2.94–29.33
data	8845	6057	6841	3761
restraints	0	1	12	0
parameters	402	381	410	180
unique reflns $I>2\sigma(R_{int})$	6100 (0.0269)	5710 (0.0595)	4798 (0.0455)	3524 (0.0212)
GOF on F^2	0.865	0.998	0.907	0.987
R_1/wR_2 ($I>2\sigma(I)$)	0.0249, 0.0483	0.0269, 0.0648	0.0441, 0.0898	0.0179, 0.0392
R_1/wR_2 (all data)	0.0435, 0.0503	0.0287, 0.0652	0.0708, 0.0966	0.0200, 0.0394
largest diff. [e Å^{-3}]	0.584/−0.338	1.209/−0.786	1.446/−1.031	0.416/−0.434

Table 2. Crystallographic data of compounds **4′c**, **5**, **6a** and **6b**.

	4′c·0.25*n* C_6H_6	**5**·*n* $C_6H_4Cl_2$	**6a**·0.5*n* $C_6H_4Cl_2$	**6b**·0.5n $C_6H_4Cl_2$
formula	$C_{11.5}H_{16.5}CuFeIP_5$	$C_{32}H_{38}Cl_4Cu_6Fe_2I_6P_{10}$	$C_{16.4}H_{22.6}Cl_{4.8}Cu_4FeN_2P_5$	$C_{17}H_{23}Br_4ClCu_4FeN_2P_5$
M_r	555.90	2128.46	882.78	1075.32
crystal size [mm]	0.09×0.07×0.05	0.13×0.10×0.01	0.28×0.04×0.02	0.21×0.03×0.01
T [K]	123(1)	123(2)	123(2)	123(2)
space group	tetragonal	monoclinic	triclinic	triclinic
crystal system	$P\bar{4}2_1c$	$P2_1/c$	$P\bar{1}$	$P\bar{1}$
a [Å]	12.1266(1)	14.4792(3)	11.487(1)	11.7422(6)
b [Å]	12.1266(1)	12.4370(2)	11.7177(7)	11.9598(6)
c [Å]	24.1882(4)	16.0120(4)	12.3200(9)	12.6192(9)
α [°]	90	90	116.751(7)	117.329(6)
β [°]	90	104.873(2)	90.766(7)	92.801(5)
γ [°]	90	90	95.423(7)	94.842(4)
V [Å^3]	3556.98(7)	2786.81(10)	1471.3(2)	1561.1(2)
Z	8	2	2	2
ρ_{calcd} [g cm^{-3}]	2.076	2.537	1.993	2.131
μ [mm^{-1}]	25.778	37.296	13.738	15.131
Θ range [°]	3.65–66.55	3.16–51.57	3.87–51.68	3.80–51.90
data	3042	3026	3199	3436
restraints	0	12	0	0
parameters	180	276	297	278
unique reflections $I>2\sigma(R_{int})$	2948 (0.0319)	1884 (0.0800)	1768 (0.0493)	2375 (0.0542)
GOF on F^2	1.046	0.959	0.944	0.950
R_1/wR_2 ($I>2\sigma(I)$)	0.0189, 0.0435	0.0647, 0.1578	0.0490, 0.1134	0.0454, 0.0967
R_1/wR_2 (all data)	0.0203, 0.0442	0.0938, 0.1667	0.0933, 0.1254	0.0682, 0.1072
largest diff. [e Å^{-3}]	0.597/−0.364	3.093/−2.254	1.150/−0.685	1.147/−0.616

ortho-dichlorobenzene molecules arranged between the Cp* ligands of neighbouring layers.[10]

*Crystal structure of **6a** and **6b***: Compounds **6a** and **6b** are isostructural and crystallize as red needles in the triclinic space group $P\bar{1}$. Figure 6 shows a section of the 1D polymeric structure of **6**. The tilted tube-like structures of **6a**,**b** are built up from two *cyclo*-P_5 ligands from **1**, which are coordinated to each other via two copper atoms. The resulting six-membered Cu_2P_4 ring (P1, P5, Cu2) contains an inversion

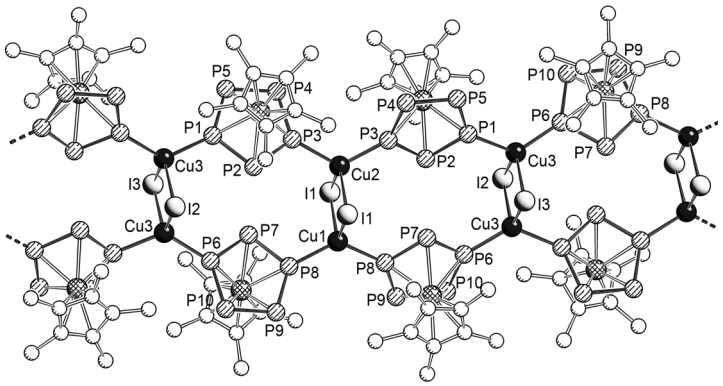

Figure 2. Section of the 1D polymeric structure of **3**. Hydrogen and carbon atoms are omitted for clarity. Selected bond lengths [Å]: P1–P2 2.110(4), P1–P5 2.113(4), P2–P3 2.106(4), P3–P4 2.112(4), P4–P5 2.126(4), P6–P7 2.095(4), P6–P10 2.123(4), P7–P8 2.100(4), P8–P9 2.109(4), P9–P10 2.118(4), Cu1–P8 2.263(3), Cu2–P3 2.257(3), Cu3–P1 2.252(3), Cu3–P6 2.260(3), Cu1–I1 2.6496(13), Cu2–I1 2.6352(13), Cu3–I2 2.6588(15), Cu3–I3 2.6415(15).

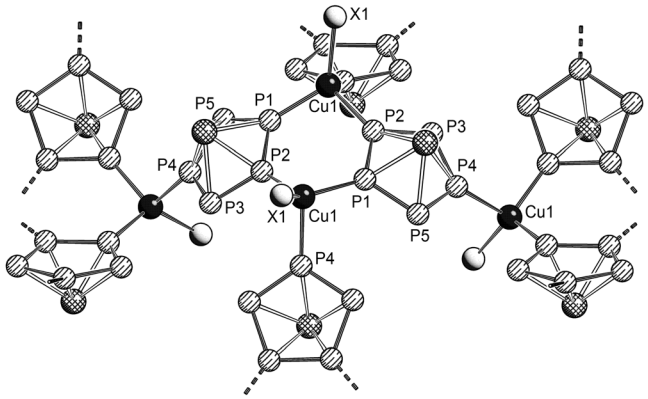

Figure 3. Section of the 2D polymeric structure of **4′** (X = Br (**4′b**), I (**4′c**)). Hydrogen atoms are omitted for clarity. Selected bond lengths [Å] for **4′b**: P1–P2 2.1098(8), P1–P5 2.1160(9), P2–P3 2.1067(9), P3–P4 2.1112(9), P4–P5 2.1139(9), Cu1–P1 2.2850(6), Cu1–P2 2.2830(6), Cu1–P4 2.3462(7), Cu1–Br1 2.3617(4); and for **4′c**: P1–P2 2.1066(12), P1–P5 2.1056(13), P2–P3 2.1136(12), P3–P4 2.1092(13), P4–P5 2.1064(12), Cu1–P1 2.2795(10), Cu1–P2 2.2847(10), Cu1–P4 2.3366(11), Cu1–I1 2.5461(5).

centre and is entirely planar. The P_5-Cu_2-P_5 unit itself is also almost planar (the torsion angles are 175.905(7) and 160.121(8)°, respectively). These central P_5-Cu_2-P_5 units are connected to each other by Cu_2P_4 six-membered rings (P2, P3, Cu3), which display a chair-like conformation (Figure 7). The phosphorus- and copper-containing polymeric backbone is coordinated by different copper halide fragments, so that three- to seven-membered rings are formed. The *cyclo*-P_5 ligand of **1** shows a rather unusual coordination mode. All P atoms of the ring are coordinated to Cu^I centres in different fashions; P1, P2, P3 and P5 coordinate in an η^1 mode to Cu atoms and additionally the P4–P5 edge coordinates to Cu4 in an η^2 mode. The latter coordination mode induces a slight elongation of the P4–P5 bond lengths (**6a**: 2.154(4) Å, **6b**: 2.162(3) Å) compared to the uncoordinated complex **1** (av.

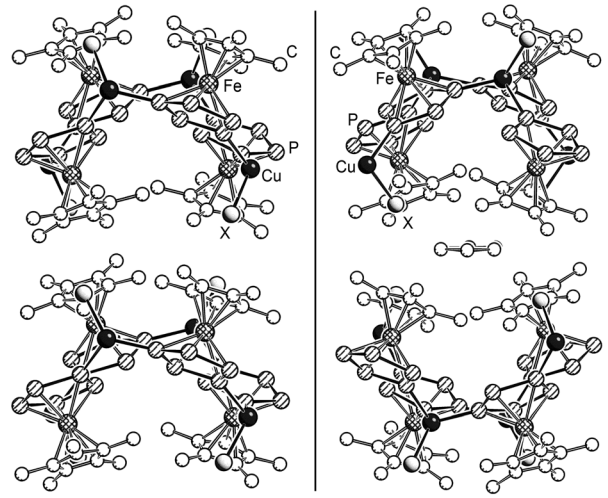

Figure 4. Comparison of the packing modes in compounds **4**; view along the crystallographic *a* axis, H atoms are omitted for clarity. The different arrangement of the undulating layers in polymers **4′b**,**c** (right) compared with **4a**,**b**,**c** (left) results in voids just big enough to host a benzene molecule.

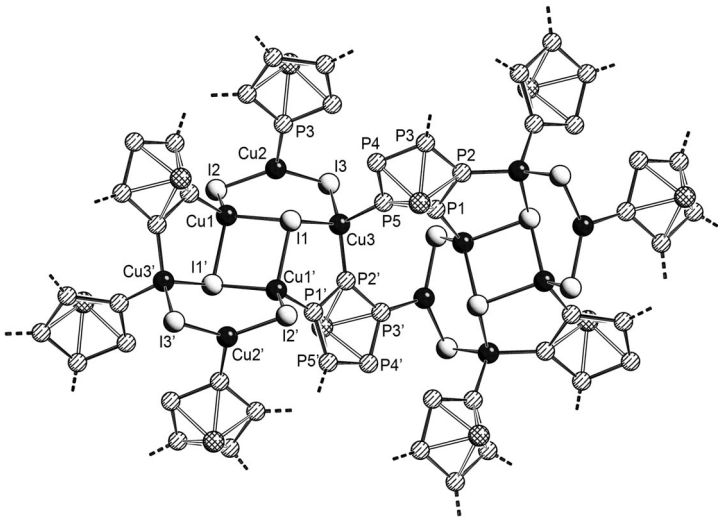

Figure 5. Section of the 2D polymeric structure of **5**. Cp* ligands are omitted for clarity. Selected bond lengths [Å]: P1–P2 2.099(7), P2–P3 2.100(7), P3–P4 2.105(7), P4–P5 2.117(7), P5–P1 2.099(7), Cu1–I1 2.609(3), Cu1–I1′ 2.832(3), Cu1–I2 2.576(3), Cu2–I2 2.531(3), Cu2–I3 2.548(3), Cu3–I1 2.680(3), Cu3–I3 2.571(3), Cu1–P1 2.256(6), Cu2–P3 2.234(6), Cu3–P2 2.260(6), Cu3–P5 2.275(6).

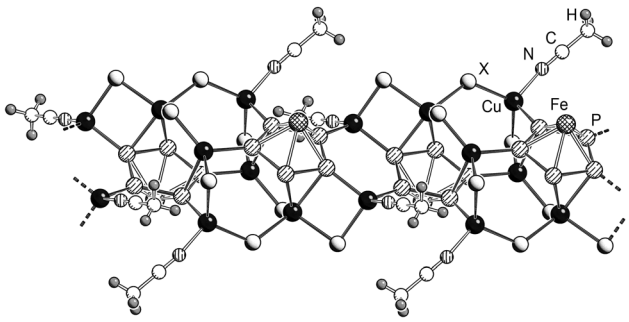

Figure 6. Section of the 1D polymeric structure of **6** (X = Cl (**6a**), Br (**6b**)). Cp* ligands are omitted for clarity.

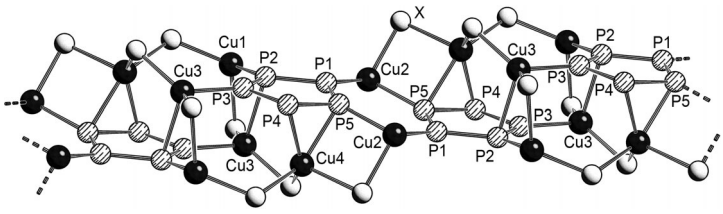

Figure 7. Section of the polymeric backbone of **6** (X = Cl (**6a**), Br (**6b**)). Selected bond lengths [Å] for **6a**: P1–P2 2.120(4), P1–P5 2.107(4), P2–P3 2.115(4), P3–P4 2.130(4), P4–P5 2.154(4), Cu1–P2 2.253(3), Cu2–P1 2.254(3), Cu2–P5 2.301(3), Cu3–P2 2.506(3), Cu3–P3 2.242(3), Cu4–P4 2.327(3), Cu4–P5 2.466(3), Cu–Cl 2.247(3)–2.425(3); and for **6b**: P1–P2 2.119(3), P1-–5 2.102(2), P2–P3 2.118(3), P3–P4 2.139(3), P4–P5 2.162(3), Cu1–P2 2.245(2), Cu2–P1 2.269(2), Cu2–P5 2.300(2), Cu3–P2 2.500(2), Cu3–P3 2.255(2), Cu4–P4 2.335(2), Cu4–P5 2.484(2), Cu–Br 2.3645(14)–2.5328(13).

2.117(4) Å).[6b,9] The π coordination to Cu3 and Cu4 proceeds with comparably long Cu–P bond lengths. The Cu3–P2 bonds (**6a**: 2.506(3) Å, **6b**: 2.500(2) Å) are the longest representatives. All copper atoms are coordinated by either three, four or five ligands. Similarly to compound **3**, *ortho*-dichlorobenzene molecules separate the polymeric chains of **6a**,**b** in the crystal lattice by forming stacks with two Cp* ligands of neighbouring strands.[10] The tubular structure of **6** with an all-P coordination to Cu is unprecedented in comparison to the kinetically controlled formation of spherical molecules observed to date, and represents an alternative route to tubular 1D polymers instead of the flat polymers found to date as the thermodynamic products with a maximum of coordination of 2, 3 or 4 P atoms of the *cyclo*-P_5 ring.

^{31}P MAS NMR spectroscopic characterization: Because the insufficient solubility of coordination polymers **2**–**6** precludes their characterization by solution-state NMR spectroscopy, high-resolution one- and two-dimensional ^{31}P solid-state NMR spectroscopic techniques have been applied for their structural analysis. As previously documented for other phosphorus-cluster-based compounds and polymers,[4b–f] the obtained spectra not only resolve all chemically and/or crystallographically inequivalent phosphorus environments but also reveal peak splitting caused by both homo- and heteronuclear indirect dipolar interactions, such as ^{31}P,^{31}P or ^{31}P,^{63,65}Cu scalar couplings. Peak assignments have been made based on intensity arguments and on the basis of cross-peaks observed in two-dimensional total-through-bond homonuclear correlation spectra, which can discriminate through-bond connectivity from mere spatial proximity. Indeed, the applied mixing times of the particularly robust and versatile R-TOBSY sequence[11] were chosen sufficiently short to ensure rather selective detection of coherences caused by one-bond (^1J) scalar spin-spin interactions. Tables 3 and 4 summarize all relevant interaction parameters, including ^{31}P chemical shifts and scalar coupling constants $^1J(^{31}P,^{31}P)$ and $^1J(^{31}P,^{63,65}Cu)$, which were extracted from lineshape simulations by using the DMFit software.[12]

Table 3. Solid-state NMR interaction parameters of compound **2a**.

	Sites	δ_{iso} [ppm]	(J_{iso}±10) [Hz]
A	P4	166.3	$J(\mathbf{A},\mathbf{C}) = 388$, $J(\mathbf{A},\mathbf{C}') = 440$
B	P1, P2	113.9	$J(\mathbf{B},\mathbf{C}) = 380$; $J(\mathbf{B},\mathbf{B}') = 353$, $J(\mathbf{B},\mathrm{Cu}) \approx 466$
	P1, P2	121.9	$J(\mathbf{B}',\mathbf{C}') = 403$; $J(\mathbf{B},\mathbf{B}') = 353$, $J(\mathbf{B}',\mathrm{Cu}) = 467$
C	P3, P5	103.8	$J(\mathbf{C},\mathbf{A}) = 388$; $J(\mathbf{C},\mathbf{B}) = 403$
	P3, P5	105.9	$J(\mathbf{C}',\mathbf{A}) = 440$, $J(\mathbf{C},\mathbf{B}) = 403$

Table 4. Solid-state NMR interaction parameters of compounds **4a**–**c**.

4a	Site	δ_{iso} [ppm]	(J_{iso}±15) [Hz]
A	P4	136.2	$^1J(\mathbf{A},\mathbf{E}) = 482$, $^1J(\mathbf{A},\mathbf{C}) = 501$, $^1J(\mathrm{P,Cu}) = 520$
B	P3 or P5	84.9	$^1J(\mathbf{B},\mathbf{E}) = 465$, $^1J(\mathbf{B},\mathbf{D}) = 522$
C	P5 or P3	75.9	$^1J(\mathbf{C},\mathbf{D}) = 470$, $^1J(\mathbf{C},\mathbf{E}) = 529$
D	P1 or P2	106.0	$^1J(\mathbf{B},\mathbf{D}) = 530$, $^1J(\mathbf{D},\mathbf{E}) = 450$, $^1J(\mathrm{P,Cu}) = 828$
E	P2 or P1	118.0	$^1J(\mathbf{C},\mathbf{E}) = 521$, $^1J(\mathbf{D},\mathbf{E}) = 447$, $^1J(\mathrm{P,Cu}) = 823$
4b	Site	δ_{iso} [ppm]	(J_{iso}±10) [Hz]
A	P4	137.0	$^1J(\mathbf{A},\mathbf{E}) = 481$, $^1J(\mathbf{A},\mathbf{C}) = 481$, $^1J(\mathrm{P,Cu}) = 559$
B	P3 or P5	80.8	$^1J(\mathbf{B},\mathbf{E}) = 481$, $^1J(\mathbf{B},\mathbf{D}) = 537$
C	P5 or P3	73.6	$^1J(\mathbf{C},\mathbf{D}) = 481$, $^1J(\mathbf{C},\mathbf{E}) = 527$
D	P1 or P2	104.5	$^1J(\mathbf{B},\mathbf{D}) = 537$, $^1J(\mathbf{D},\mathbf{E}) = 476$, $^1J(\mathrm{P,Cu}) = 783$
E	P2 or P1	115.3	$^1J(\mathbf{C},\mathbf{E}) = 527$, $^1J(\mathbf{D},\mathbf{E}) = 476$, $^1J(\mathrm{P,Cu}) = 787$
4c	Site	δ_{iso} [ppm]	(J_{iso}±10) [Hz]
A	P3	135.7	$^1J(\mathbf{A},\mathbf{B}) = 438$, $^1J(\mathrm{P,Cu}) = 545$
B	P2	75	$^1J(\mathbf{A},\mathbf{B}) = 438$, $^1J(\mathbf{B},\mathbf{C}) = 518$
C	P1	102.8	$^1J(\mathbf{C},\mathbf{B}) = 518$; $^1J(\mathrm{P,Cu}) = 763$

Figure 8 shows the ^{31}P MAS NMR spectrum of compound **2a**. Three groups of multiplets are visible, corresponding to the three chemically different types of phosphorus species present in the *cyclo*-P_5 ring. Based on the spectral intensity, the signal centred at $\delta = 166.3$ ppm must be assigned to P4. The best possible fit includes a slight difference in the ^1J scalar coupling constants to the crystallographically inequi-

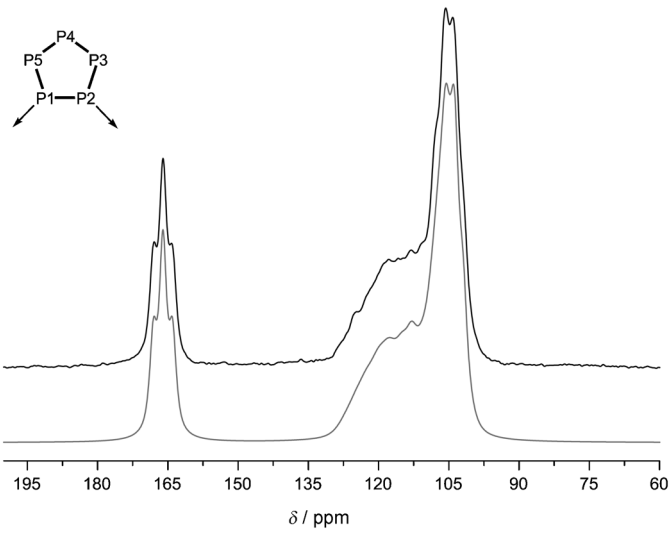

Figure 8. ^{31}P MAS NMR spectrum of the compound **2a** [CuCl-{Cp*Fe(μ,η⁵:η¹:η¹-P_5)}]$_\infty$ at 11.7 T (202.49 MHz) and a spinning frequency of 30 kHz with 10 s relaxation delay, acquiring 4096 scans. The grey curve represents a spectral simulation based on the parameters listed in Table 3.

valent P3 and P5 sites, which also show a minor difference in their chemical shifts. Likewise, the two P1 and P2 sites have a small difference in chemical shift, and their spectrum forms a poorly resolved envelope broadened by both $^{1}J(^{31}P,^{31}P)$ and $^{1}J(^{31}P,^{63,65}Cu)$ spin–spin couplings, respectively. The two-dimensional homonuclear correlation spectrum, obtained by using the R-TOBSY method, is shown in Figure 9.

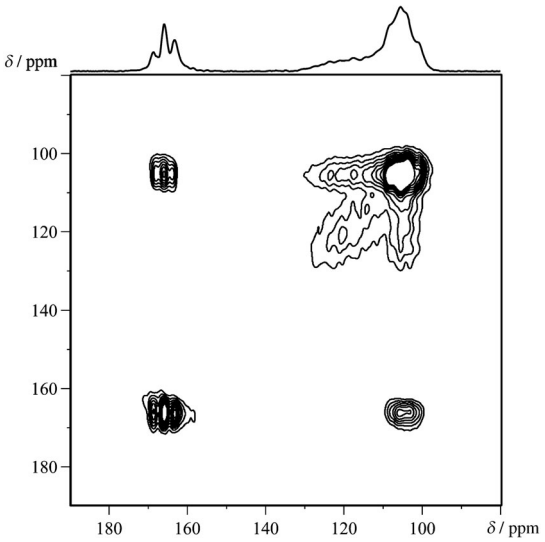

Figure 9. 25 kHz ^{31}P MAS NMR R-TOBSY spectrum of [CuCl-{Cp*Fe(μ,η^5:η^1:η^1-P$_5$)}]$_n$ **2a** at 9.4 T (162.09 MHz), measured under the following experimental conditions: $\tau_{(mix)} = 0.32$ ms, 62 t_1 increments at steps of 40 μs, relaxation delay 10 s. Ten positive contour levels between 5 and 50 % of the maximum peak intensity are plotted. The F_2 projection is shown on the top.

From this spectrum it is evident that the multiplet centred at about 105 ppm must be assigned to P3 and P5 because it is the only site that reveals cross-peaks with both of the other ^{31}P resonances. The overall appearance of this resonance as a doublet of doublets arises from the $\delta \approx 1$ ppm difference in chemical shifts, which reflects the crystallographic inequivalence of both P3 and P5 and the difference in ^{1}J coupling constants to P4. Finally, the multiplet centred around $\delta =$ 118 ppm is attributed to P1 and P2. The indirect spin–spin interaction with the four Zeeman states of the ^{63,65}Cu isotopes is only poorly resolved, but together with the moderate chemical shift difference contributes to the overall breadth of the signal envelope. In addition, further broadening due to residual heteronuclear ^{31}P,^{63,65}Cu dipolar coupling cannot be excluded, given that the copper atom is located at the centre of a strongly distorted tetrahedron in which copper–chlorine interactions produce an exceptionally large anisotropy and thus impose characteristic lineshapes of strong second-order quadrupolar perturbations on the corresponding ^{63}Cu MAS NMR spectrum of **2a** (data not shown).

Figure 10 displays the one-dimensional spectra of compound **4b**. A good fit to the experimental data can be obtained based on five distinct resonances that represent all crystallographically inequivalent sites in the P_5 molecule.

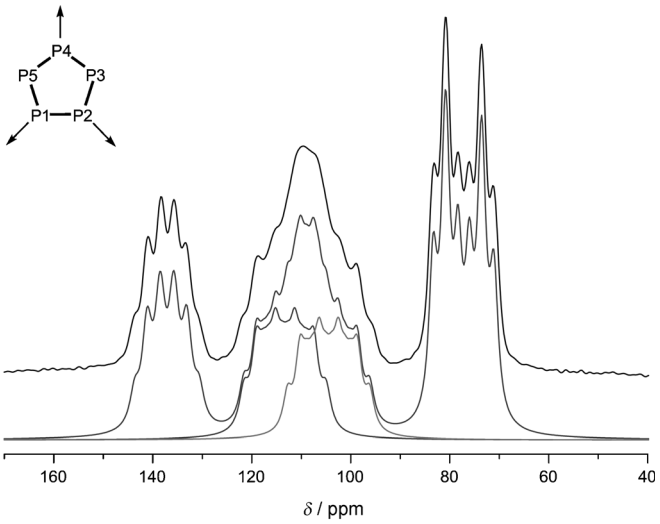

Figure 10. Experimental (top) and simulated (bottom) ^{31}P MAS NMR spectrum of [CuBr{Cp*Fe(μ,η^5:η^1:η^1:η^1-P$_5$)}]$_n$ **4b** at 11.7 T (202.45 MHz) and a spinning frequency of 30 kHz with 16 s relaxation delay, acquiring 4096 scans. The superimposed grey curve is a spectral simulation based on the parameters listed in Table 3, in which the two sites that comprise the broad signal are highlighted.

Based on the spectral intensity, the signal centred at $\delta =$ 136 ppm is assigned to the unique P4 site, at which peak multiplicity arising from indirect spin–spin coupling to both the ^{63}Cu and ^{65}Cu nuclei and adjacent nuclei P3 and P5 is only partially resolved. These phosphorus species give rise to the triplets observed at the lowest ppm values, as evidenced by the absence of scalar interactions with copper isotopes. Indeed, this peak assignment is corroborated by the corresponding R-TOBSY spectrum of **4b**, which reveals cross-peaks with all of the other groups of resonances (Figure 11). This two-dimensional spectrum, however, lacks spectral resolution to reliably distinguish between the individual connectivity patterns of those two phosphorus species. The rather broad signal centred around $\delta = 110$ ppm must be assigned to P1 and P2, for which the considerable breadth of the envelope arises from a combination of a $\delta =$ 11 ppm chemical shift difference between both resonances and hetero-nuclear scalar coupling between phosphorus and the copper isotope nuclei. An analogous spectrum is observed for compound **4a** except that the chemical shift differences among the same groups of spins are even larger (Figure 12). The 2D spectrum (Figure 13) confirms the close analogy to compound **4b**. In this case, the resolution is sufficient for differentiating the individual connectivity patterns P2–P3 and/or P1–P5, even though the final ambiguity as to whether the signal at the lowest frequency can be assigned to P3 or P5 cannot be removed. Furthermore, in contrast to the situation in compound **4b** (Figure 11), the 2D R-TOBSY spectrum of compound **4a** reveals cross-peaks arising from the P1–P2 connectivity because they are better resolved from the diagonal owing to the larger chemical shift difference.

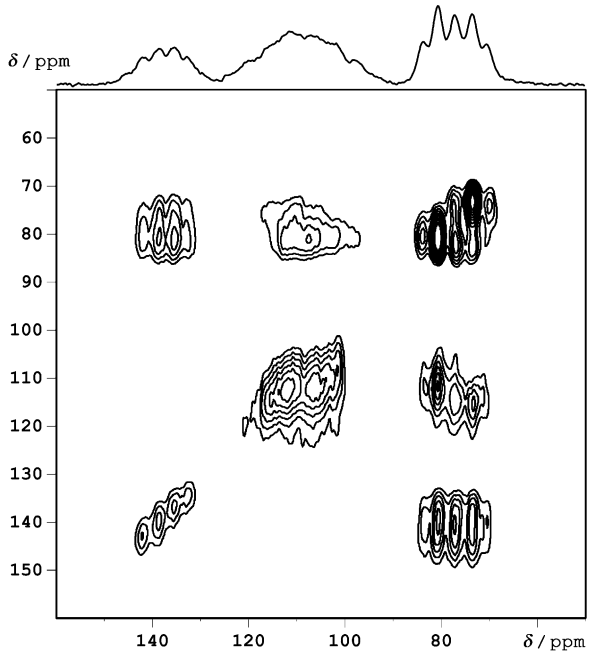

Figure 11. 30 kHz ^{31}P MAS NMR R-TOBSY spectrum of [CuBr{Cp*Fe(μ,η^5:η^1:η^1-P_5)}]$_n$ **4b** at 11.7 T (202.45 MHz) under the following experimental conditions: $\tau_{(mix)}$ = 0.49 ms, 110 t_1 increments at steps of 11.11 μs, relaxation delay 16 s. Ten positive contour levels between 18 and 68 % of the maximum peak intensity are plotted. The F_2 projection is shown on the top.

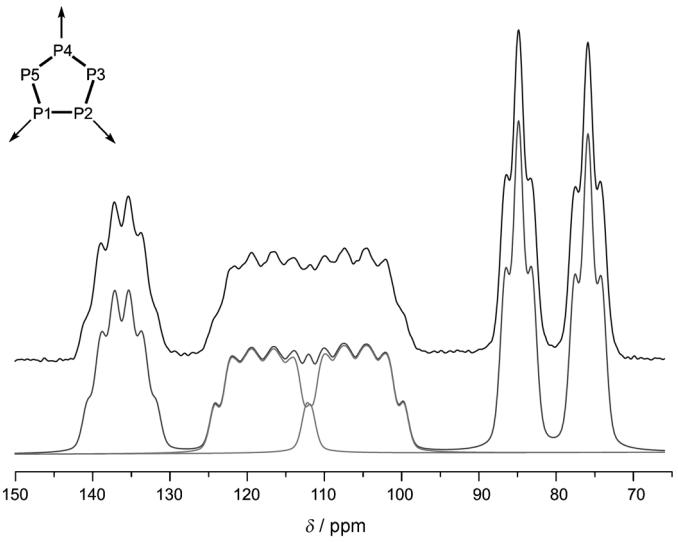

Figure 12. Experimental (top) and simulated (bottom) ^{31}P MAS NMR spectrum of [CuCl{Cp*Fe(μ,η^5:η^1:η^1-P_5)}]$_n$ **4a** at 16.4 T (283.41 MHz) and a spinning frequency of 25 kHz, with 30 s relaxation delay, acquiring 4096 scans. The superimposed grey curve is a spectral simulation based on the parameters listed in Table 3, in which the two sites that comprise the broad signal are further highlighted.

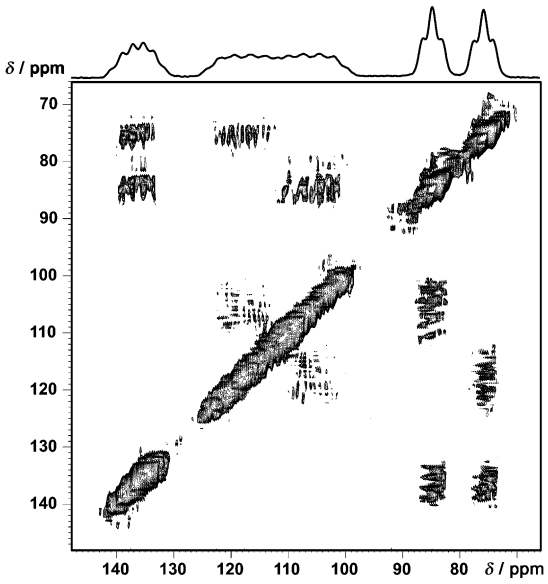

Figure 13. 25 kHz ^{31}P MAS NMR R-TOBSY spectrum of [CuCl{Cp*Fe(η^5:η^1:η^1-P_5)}]$_n$ **4a** at 16.4 T (283.41 MHz) and a spinning frequency of 25 kHz, under the following experimental conditions: $\tau_{(mix)}$ = 0.96 ms, 88 t_1 increments at steps of 40 μs, relaxation delay 40 s. Sixteen positive contour levels between 5 and 73 % of the maximum peak intensity were plotted. The F_2 projection is shown on the top. The spectrum was symmetrized by using the Bruker Topspin 2.1 software.

(Figure 14). Based on the R-TOBSY spectra (Figure 15), these signals can be clearly assigned to the different P atoms that comprise the asymmetric unit of the crystal structure.

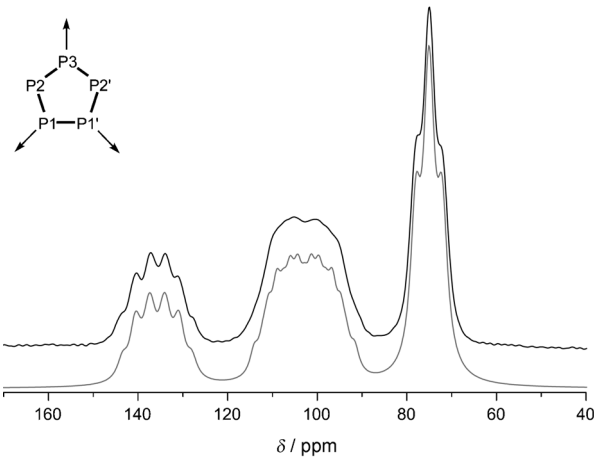

Figure 14. ^{31}P MAS NMR spectrum of [CuI{Cp*Fe(μ,η^5:η^1:η^1-P_5)}]$_n$ **4c** at 11.7 T (202.49 MHz) and a spinning frequency of 30 kHz. The superimposed grey curve is a spectral simulation based on the parameters listed in Table 3.

In compound **4c**, only three crystallographically distinct phosphorus species are refined, which thus indicates that the *cyclo*-P_5 ring possesses C_2 symmetry. In good agreement with this finding, only three ^{31}P MAS NMR signals are visible in the corresponding solid-state NMR spectrum

Table 4 summarizes the chemical shifts and *J* coupling constants extracted from simulations of the ^{31}P MAS NMR spectra of compounds **4a–c**.

Figure 16 shows the one-dimensional ^{31}P MAS NMR spectrum of **5**, which reveals three resonances with distinct

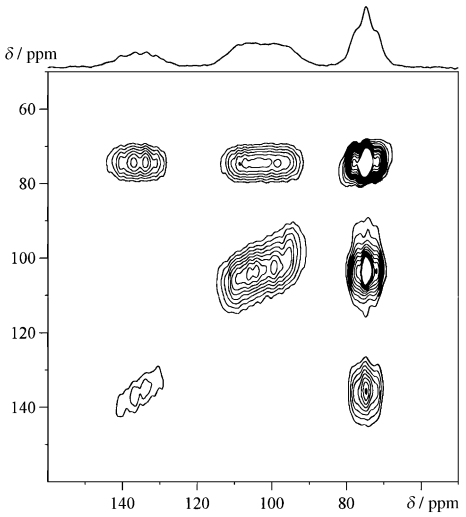

Figure 15. 30 kHz ^{31}P MAS NMR R-TOBSY spectrum of $[CuI\{Cp^*Fe(\mu,\eta^5{:}\eta^1{:}\eta^1{:}\eta^1\text{-}P_5)\}]_n$ **4c** at 9.4 T (162.02 MHz), under the following experimental conditions: $\tau_{(mix)} = 0.48$ ms, 146 t_1 increments at steps of 33.33 μs, relaxation delay 10 s.

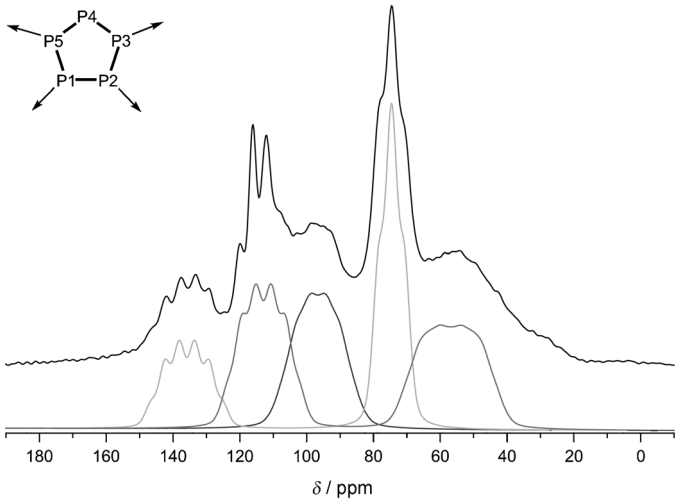

Figure 16. ^{31}P MAS NMR spectrum of $[\{Cu_3(\mu\text{-}I)_2(\mu_3\text{-}I)\}\{Cp^*Fe(\mu_5,\eta^5{:}\eta^1{:}\eta^1{:}\eta^1{:}\eta^1\text{-}P_5)\}]_n$ **5** at 7.0 T (121.5 MHz) and a spinning frequency of 30 kHz. Tentative simulation parameters of the individual spectral components are $\delta = 135.86$ ppm, $^1J(P,Cu) = 556$ Hz, $^1J(P,P) = 475$ Hz (×2); $\delta = 112.94$ ppm, $J(P,Cu) = 556$ Hz, $^1J(P,P) = 475$ Hz (×2); $\delta = 96.64$ ppm, $J(P,Cu) = 556$ Hz, $^1J(P,P) = 475$ Hz (×2); $\delta = 74.58$ ppm, $^1J(P,P) = 475$ Hz (×2); $\delta = 56.87$ ppm, $J(P,Cu) = 780$ Hz, $^1J(P,P) = 475$ Hz (×2).

scalar spin–spin coupling patterns. A best-effort simulation attempt indicates unaccounted-for signal intensity near $\delta =$ 118 ppm and in the $\delta = 30$ to 50 ppm range, which suggests the presence of some impurities. Based on the absence of J splitting to ^{63,65}Cu isotopes, the signal near $\delta = 75$ ppm must be attributed to P4, which is the only phosphorous atom devoid of P–Cu bonding (for assignments of the P atoms, see Figure 5). For all other signals unambiguous assignment is not possible because the corresponding R-TOBSY measurements did not give satisfactory results owing to extremely long spin-lattice relaxation times.

Finally, the spectrum of compound **6a**, in which all the P atoms are connected to Cu, only exhibits a broad, weakly structured lineshape extending from $\delta = 40$ to 140 ppm and without significant peak resolution (data not shown).[10] The excessive line broadening observed in this case most likely reflects strong direct and indirect ^{31}P–^{63,65}Cu dipolar interactions that affect the ^{31}P resonances of all phosphorus sites in the *cyclo*-P_5 ring. For this reason no 2D NMR spectroscopy was attempted. Thus, ^{31}P MAS NMR spectroscopy is unable to differentiate between the above-described different P–Cu coordination modes in this case.

Although the reaction of **1** with Cu^I halides results in insoluble 1D or 2D polymeric compounds with rather static "fixation" of the *cyclo*-P_5 ring in the solid aggregation state, the corresponding reaction with Ag^I salts of the weakly coordinating anion $[Al\{OC(CF_3)_3\}_4]^-$ results in a 1D polymer[6b] in the solid state, which shows a depolymerization on redissolving the product in polar solvents, such as CH_2Cl_2. In this case, monomer–oligomer equilibria were detected by using solution NMR spectroscopy whereas the 1,2,3 coordination mode **C** identified in solid $[Ag\{Cp^*Fe(\eta^5{:}\eta^2{:}\eta^1\text{-}P_5)\}_2]_n[Al\{OC(CF_3)_3\}_4]_n$ (**7**) was further investigated by using ^{31}P MAS NMR spectroscopy (see Figure 17). However, this 1,2,3 coordination mode is not symmetric because the P1–P2 edge binds to one Ag site in a η^2 mode and the P3 atom to

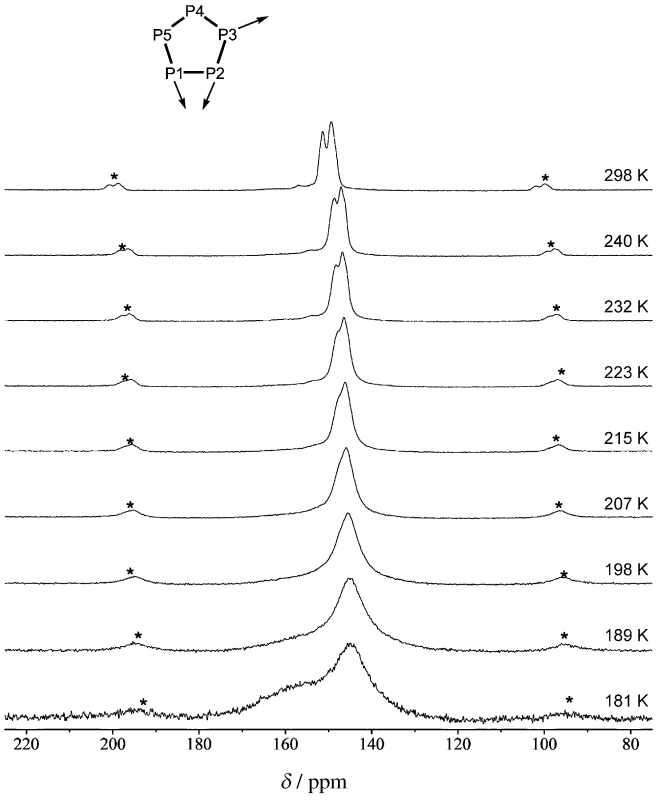

Figure 17. ^{31}P MAS NMR spectra of compound $[Ag\{Cp^*Fe(\eta^5{:}\eta^2{:}\eta^1\text{-}P_5)\}_2]_n[Al\{OC(CF_3)_3\}_4]_n$ (**7**) at different temperatures.

another Ag site in an η^1 mode. Therefore, five different P sites are expected in **7** with a 1:1:1:1:1 integrated area ratio. Furthermore, two types of *cyclo*-P_5 rings are present in the polymeric chains of **7**, which are crystallographically different due to the different number of neighbouring counterions.[10] The room-temperature ^{31}P MAS NMR spectrum of **7** exhibits two relatively narrow resonances at about $\delta = 148$ and 152 ppm in an approximate 2:1 ratio, in addition to a small shoulder extending towards $\delta = 155$ ppm. Notably, unambiguous peak assignment is not straightforward, in particular due to the likely presence of molecular motion, such as rotational processes. Upon decreasing the temperature, the ^{31}P MAS NMR spectral line-shapes broaden significantly to give two peak contributions centred near $\delta = 145$ and 155 ppm. Line-broadening phenomena of this kind are typically observed in MAS NMR spectra as a result of molecular dynamic processes occurring at rates comparable to the MAS spinning rate. In the present compound the room-temperature spectrum cannot be attributed to a simple axial rotation of the *cyclo*-P_5 rings because the latter would produce equivalent local environments for all of the P nuclei of the *cyclo*-P_5 unit, and thus would show two signals for the two crystallographically different P_5 rings in 1:1 ratio. Rather, the temperature-dependent ^{31}P MAS NMR spectra suggest more complex reorientational processes of the *cyclo*-P_5 units.

Conclusion

We have shown that, upon modification of the reaction conditions (different solvent mixtures, stoichiometry and third reaction component) in the reaction between Cu^I halides and [Cp*Fe(η^5-P_5)] (**1**), novel polymeric compounds are accessible. These compounds give a series of 1D and 2D polymeric compounds that exhibit unprecedented coordination patterns of the *cyclo*-P_5 ring of pentaphosphaferrocene **1**. Besides the previously reported 1,2 and 1,2,4 coordination modes at this ring, novel 1,3 and 1,2,3,4 coordination patterns were identified in the obtained polymers. Notably, in some cases inclusion of solvent molecules resulted in different packing modes of the polymeric strands. In addition, some of the products have been successfully prepared by using $CuCl_2$ and $CuBr_2$, respectively, which led to Cu^I-containing polymers as a result of proceeding redox processes. Moreover, the unprecedented 1D tubular polymers **6a**,**b** could be isolated successfully, and reveal entire coordination of all available phosphorous atoms to Lewis-acidic Cu centres. These products represent a structural alternative to the kinetically stable spherical supramolecules also formed by these systems.

By applying high-resolution one- and two-dimensional ^{31}P solid-state MAS NMR spectroscopic techniques, including R-TOBSY experiments, ^{31}P,^{31}P and/or ^{31}P,^{63,65}Cu scalar coupling constants and peak assignment of selected compounds have been obtained. The results are convincing, particularly in those compounds that contain the *cyclo*-P_5 ring in 1,2 or 1,2,4 coordination modes. Based on these results, a more rational analysis of particular scalar coupling patterns in as-yet unknown compounds that contain a *cyclo*-P_5 unit is possible. However, in products with four P atoms coordinating to Cu, the assignment by MAS NMR spectroscopic analyses becomes rather difficult, and in the case of a polymer with all 5 P atoms coordinating to Cu atoms the results were rather inconclusive. Finally, ^{31}P MAS spectroscopic analyses of Ag complex **7** show dynamic behaviour of the *cyclo*-P_5 ring even in the solid state, which could not be resolved at lower temperatures.

The presented results provide a striking demonstration of how small changes in reaction conditions can have a decisive impact on the supramolecular self-assembly processes, and furthermore show the power of advanced solid-state NMR spectroscopic methods for the analysis of coupling patterns.

Experimental Section

General: All manipulations were carried out under an atmosphere of nitrogen or argon by using standard Schlenk techniques. All solvents were dried by using standard procedures and freshly distilled before use. [Cp*Fe(η^5-P_5)] (**1**),[13] **2a**,[6a] **4a**,[7a] **4b**[6a] and **4c**[6a] were prepared according to literature procedures.

[{Cu(μ-Cl)}{Cp*Fe(μ_3,η^5:η^1:η^1-P_5)}]$_n$·0.5*n* C_6H_6 (2a·0.5*n* C_6H_6): A solution of $CuCl_2$ (12 mg, 0.087 mmol) in CH_3CN (10 mL) was layered onto a solution of [Cp*Fe(η^5-P_5)] (**1**; 30 mg, 0.087 mmol) in benzene (10 mL) at RT. After complete diffusion of the solvent mixture, green crystals of **2a** were isolated. The mother liquor was decanted and the obtained crystals were washed three times with hexane and dried under vacuum (16 mg, 41%). Elemental analysis calcd (%) for $C_{26}H_{36}Cl_2Cu_2Fe_2P_{10}$: C 32.26, H 3.75; found: C 32.21, H 3.58.

[{Cu(μ-I)}{Cp*Fe(μ_3,η^5:η^1:η^1-P_5)}]$_n$·0.5*n* THF (2′c·0.5*n* THF): A solution of CuI (28 mg, 0.15 mmol) in a mixture of CH_3CN (5 mL) and THF (5 mL) was layered onto a solution of [Cp*Fe(η^5-P_5)] (**1**; 26 mg, 0.075 mmol) in THF (10 mL) at RT. After complete diffusion of the solvent mixture, black needles of **2′c** were formed. The mother liquor was decanted and the remaining crystals were washed with pentane and dried under vacuum (13 mg, 47.3%). Elemental analysis calcd (%) for $C_{20}H_{30}I_2Cu_2Fe_2P_{10}$: C 22.39, H 2.82; found: C 22.02, H 2.21.

[{CuI}{Cp*Fe(η^5:η^1:η^1-P_5)}]$_n$·0.5*n* $C_6H_4Cl_2$ (3·0.5*n* $C_6H_4Cl_2$): A solution of CuI (55 mg, 0.29 mmol) in CH_3CN (10 mL) was carefully layered onto a solution of [Cp*Fe(η^5-P_5)] (**1**; 50 mg, 0.145 mmol) and [$CoCp_2$] (15 mg, 0.08 mmol) in *ortho*-dichlorobenzene (10 mL) at RT. After complete diffusion of the solvent mixture, two different kinds of crystals were formed: brown elongated blocks of **3** and red plates of a spherical compound (the composition of which could not be determined). The mother liquor was decanted and the obtained crystals were washed with pentane and dried under vacuum. Crystals of **3** could be separated by using a microscope in a dry box (19 mg, 11%). The compound was not sufficiently pure for MAS-NMR spectroscopic analyses.

[{CuBr}{Cp*Fe(μ_4,η^5:η^1:η^1:η^1-P_5)}]$_n$·0.25*n* C_6H_6 (4′b·0.25*n* C_6H_6): A solution of $CuBr_2$ (19 mg, 0.087 mmol) in CH_3CN (10 mL) was layered onto a solution of [Cp*Fe(η^5-P_5)] (**1**; 30 mg, 0.087 mmol) in benzene (10 mL) at RT. After complete diffusion of the solvent mixture, brown plates of **4′b** were formed. The mother liquor was decanted and the obtained crystals were washed three times with hexane and dried under vacuum (20 mg, 47%). Elemental analysis calcd (%) for $C_{46}H_{66}Br_4Cu_4Fe_4P_{20}$ (2035.69): C 27.14, H 3.27; found: C 26.37, H 3.01.

[{CuI}{Cp*Fe(μ_4,η^5:η^1:η^1:η^1-P_5)}]$_n$·0.25*n* C_6H_6 (4′c·0.25*n* C_6H_6): A solution of CuI (17 mg, 0.087 mmol) in CH_3CN (5 mL) was layered onto a solution of [Cp*Fe(η^5-P_5)] (**1**; 30 mg, 0.087 mmol) in benzene (10 mL) at RT. During the diffusion of the solvent mixture, yellow plates that were not

suitable for single crystal X-ray analyses formed. After complete diffusion, brown blocks of **4′c** could be isolated. The mother liquor was decanted and the obtained crystals were washed three times with pentane and dried under vacuum (30 mg, 50.6%). Elemental analysis calcd (%) for $C_{46}H_{66}I_4Cu_4Fe_4P_{20}$: C 24.85, H 2.99; found: C 24.95, H 2.70.

$[\{Cu_3(\mu\text{-}I)_2(\mu_3\text{-}I)\}\{Cp^*Fe(\mu_5,\eta^5\text{:}\eta^1\text{:}\eta^1\text{:}\eta^1\text{:}\eta^1\text{-}P_5)\}]_n \cdot n\,C_6H_4Cl_2$ ($5\cdot n\,C_6H_4Cl_2$): A solution of CuI (57 mg, 0.30 mmol) in a mixture of CH_3CN (10 mL) and *ortho*-dichlorobenzene (10 mL) was layered onto a solution of $[Cp^*Fe(\eta^5\text{-}P_5)]$ (**1**; 52 mg, 0.15 mmol) in *ortho*-dichlorobenzene (10 mL) at RT. During the diffusion, a voluminous green precipitate formed, which dissolved during the further reaction, and after complete diffusion of the solvent mixture orange-red crystals of **5** were formed. The mother liquor was decanted and the obtained orange-red crystals were washed with pentane and dried under vacuum (83 mg, 53%). Elemental analysis calcd (%) for $C_{32}H_{38}Cl_4I_6Cu_6Fe_2P_{10}$: C 18.06, H 1.80; found: C 18.56, H 2.05.

$[\{Cu_4(\mu\text{-}Cl)_4(CH_3CN)\}\{Cp^*Fe(\mu_7,\eta^5\text{:}\eta^2\text{:}\eta^1\text{:}\eta^1\text{:}\eta^1\text{:}\eta^1\text{:}\eta^1\text{-}P_5)\}]_n \cdot 0.5n\,C_6H_4Cl_2$ ($6\mathbf{a}\cdot 0.5n\,C_6H_4Cl_2$): A solution of CuCl (69 mg, 0.69 mmol) in a mixture of CH_3CN (5 mL) and *ortho*-dichlorobenzene (5 mL) was layered onto a solution of $[Cp^*Fe(\eta^5\text{-}P_5)]$ (**1**; 60 mg, 0.18 mmol) in *ortho*-dichlorobenzene (10 mL) at RT. During the diffusion, orange-red plates that were not suitable for single crystal X-ray structural analyses formed. After complete diffusion, red needles of **6a** were formed. The mother liquor was decanted and the obtained crystals were washed with a mixture of acetonitrile and CH_2Cl_2 (in which the orange-red plates dissolve) and the remaining crystals of **6a** were washed three times with pentane and dried under vacuum (29 mg, 18%). Elemental analysis calcd (%) for $C_{14}H_{21}Cl_4Cu_4FeN_2P_5$: C 22.31, H 2.58, N 3.17; found: C 22.31, H 2.98, N 3.53.

$[\{Cu_4(\mu\text{-}Br)_4(CH_3CN)\}\{Cp^*Fe(\mu_7,\eta^5\text{:}\eta^2\text{:}\eta^1\text{:}\eta^1\text{:}\eta^1\text{:}\eta^1\text{:}\eta^1\text{-}P_5)\}]_n \cdot 0.5n\,C_6H_4Cl_2$ ($6\mathbf{b}\cdot 0.5n\ C_6H_4Cl_2$): A solution of CuBr (31.2 mg, 0.164 mmol) in a mixture of CH_3CN (5 mL) and *ortho*-dichlorobenzene (5 mL) was layered onto a solution of $[Cp^*Fe(\eta^5\text{-}P_5)]$ (**1**; 60 mg, 0.18 mmol) and C_{70} (10 mg, 0.01 mmol) in *ortho*-dichlorobenzene (10 mL) at RT. After complete diffusion of the phases, red rods of **6b** and dark red crystals of an as-yet unknown product were formed. The mother liquor was decanted and the obtained crystals were washed with pentane and dried under vacuum (31 mg, 47.3%).

MAS-NMR measurements: Solid-state ^{31}P MAS NMR spectroscopy studies were conducted by using Bruker Avance 300, 400, 500 or 700 spectrometers, each equipped with a commercially available Bruker 2.5 mm MAS NMR probe, which was operated at spinning speeds between 25 and 30 kHz. Typical acquisition parameters are given in the figure captions of both the one- and two-dimensional spectra. All spectra were recorded at RT and ^{31}P chemical shifts are reported relative to an 85% H_3PO_4 solution with $CaHPO_4\cdot 2H_2O$ as a secondary standard ($\delta =$ 1.4 ppm). Peak assignments were established on the basis of connectivity studies by employing the previously described R-TOBSY sequence, which belongs to the family of symmetry-based windowless recoupling sequences[14] that specifically utilize bond-mediated scalar rather than through-space homonuclear dipolar couplings to achieve coherence transfer between directly bonded nuclei. Quadrature detection in the F_1 dimension was achieved by the hyper-complex approach (STATES method).

Crystal structure determination: The crystal structure analyses were performed by using an Oxford Diffraction Gemini R Ultra CCD with Cu radiation ($\lambda = 1.54178$ Å). Semi-empirical absorption corrections from equivalents (multi-scan) were applied.[15] The structures were solved by direct methods with the program SIR-97,[16] and full matrix least-square refinement on F^2 in SHELXL-97[17] was performed. Hydrogen atoms were calculated from geometry and refined isotropically by applying the riding model. In the acentric space groups of **2c** and **3**, the molecules didn′t crystallize in an enantiomerically pure form, therefore, the Flack parameters were found to be 0.425(3) for **2′c** and 0.482(8) for **3**. The refinements of the disordered solvent molecules in **3** and **5** required the use of some restraints, which resulted in increased quality factors for **5**. Further crystallographic details are summarized in Tables 1 and 2. CCDC-831768 (**2a**), -831769 (**2′c**), -831770 (**3**), -831771 (**4′b**), -831772 (**4′c**), -831773 (**5**), -831774 (**6a**) and -831775 (**6b**) contain the supplementary crystallographic data for this paper. These data can be obtained free of charge from The Cambridge Crystallographic Data Centre via www.ccdc.cam.ac.uk/data_request/cif.

Acknowledgements

Funding by the Deutsche Forschungsgemeinschaft (projects Sche 384/26-1 and Ec168/10, "Supramolecular Aggregations") is most gratefully acknowledged. The authors are grateful to the COST action CM0802 (PhoSciNet) for general support. F.D. thanks the Studienstiftung des Deutschen Volkes for a PhD fellowship.

[1] For recent review articles, see: a) M. Yoshizawa, J. K. Klosterman, M. Fujita, *Angew. Chem.* **2009**, *121*, 3470–3490; *Angew. Chem. Int. Ed.* **2009**, *48*, 3418–3438; b) B. H. Northrop, Y.-R- Zheng, K.-W. Chi, P. J. Stang, *Acc. Chem. Res.* **2009**, *42*, 1554–1563; c) H. Furukawa, J. Kim, N. W. Ockwig, M. O'Keeffe, Q. M. Yaghi, *J. Am. Chem. Soc.* **2008**, *130*, 11650–11661; d) S. J. Dalgarno, N. P. Power, J. L. Atwood, *Coord. Chem. Rev.* **2008**, *252*, 825–841; e) K. Biradha. M. Sarkar, L. Rajput, *Chem. Commun.* **2006**, 4169–4179; f) W. Huang, H.-B. Zhu, S.-H. Gou, *Coord. Chem. Rev.* **2006**, *250*, 414–423; g) N. C. Gianneschi, M. S. Masar III, C. A. Mirkin, *Acc. Chem. Res.* **2005**, *38*, 825–837; h) M. H. Chisholm, N. J. Patmore, *Acc. Chem. Res.* **2007**, *40*, 19–27; i) M. Ruben, F. Rojo, F. J. Romero-Salguero, L. H. Uppadine, J.-M. Lehn, *Angew. Chem.* **2004**, *116*, 3728; *Angew. Chem. Int. Ed.* **2004**, *43*, 3644.

[2] M. Scheer, *Dalton Trans.* **2008**, 4372–4386.

[3] a) M. Pronold, M. Scheer, J. Wachter, M. Zabel, *Inorg. Chem.* **2007**, *46*, 1396; b) L. J. Gregoriades, G. Balázs, E. Brunner, C. Gröger, J. Wachter, M. Zabel, M. Scheer, *Angew. Chem.* **2007**, *119*, 6070; *Angew. Chem. Int. Ed.* **2007**, *46*, 5966; c) A. Biegerl, E. Brunner, C. Gröger, M. Scheer, J. Wachter, M. Zabel, *Chem. Eur. J.* **2007**, *13*, 9270; d) M. Bodensteiner, M. Dušek, M. M. Kubicki, M. Pronold, M. Scheer, J. Wachter, M. Zabel, *Eur. J. Inorg. Chem.* **2010**, 5298–5303; e) C. Gröger, H. R. Kalbitzer, W. Meier, M. Pronold, M. Scheer, J. Wachter, M. Zabel, *Inorg. Chim. Acta* **2011**, *370*, 191–197; f) C. Gröger, H. R. Kalbitzer, M. Pronold, D. Piryazev, M. Scheer, J. Wachter, A. Virovets, M. Zabel, *Eur. J. Inorg. Chem.* **2011**, 785–793.

[4] a) J. Bai, E. Leiner, M. Scheer, *Angew. Chem.* **2002**, *114*, 820–823; *Angew. Chem. Int. Ed.* **2002**, *41*, 783–786; b) M. Scheer, L. J. Gregoriades, M. Zabel, J. Bai, I. Krossing, G. Brunklaus, H. Eckert, *Chem. Eur. J.* **2008**, *14*, 282; c) M. Scheer, L. J. Gregoriades, M. Zabel, M. Sierka, L. Zhang, H. Eckert, *Eur. J. Inorg. Chem.* **2007**, 2775; d) M. Scheer, L. J. Gregoriades, J. Bai, M. Sierka, G. Brunklaus, H. Eckert, *Chem. Eur. J.* **2005**, *11*, 2163; e) S. Reiser, G. Brunklaus, J. H. Hoy, J. C. C. Chan, H. Eckert, A. Pfitzner, *Chem. Eur. J. C* **2002**, *8*, 4228; f) G. Brunklaus, J. C. C. Chan, H. Eckert, S. Reiser, T. Nilges, A. Pfitzner, *Phys. Chem. Chem. Phys.* **2003**, *5*, 3768.

[5] L. J. Gregoriades, B. K. Wegley, M. Sierka, E. Brunner, C. Gröger, E. V. Peresypkina, A. V. Virovets, M. Zabel, M. Scheer, *Chem. Asian J.* **2009**, *4*, 1578–1587.

[6] a) J. Bai, A. V. Virovets, M. Scheer, *Angew. Chem.* **2002**, *114*, 1808; *Angew. Chem. Int. Ed.* **2002**, *41*, 1737; b) M. Scheer, L. J. Gregoriades, A. V. Virovets, W. Kunz, R. Neueder, I. Krossing, *Angew. Chem.* **2006**, *118*, 5818; *Angew. Chem. Int. Ed.* **2006**, *45*, 5689; c) S. Welsch, L. J. Gregoriades, M. Sierka, M. Zabel, A. V. Virovets, M. Scheer, *Angew. Chem.* **2007**, *119*, 9483; *Angew. Chem. Int. Ed.* **2007**, *46*, 9323.

[7] a) S. Welsch, C. Gröger, M. Sierka, M. Scheer *Angew. Chem.* **2011**, *123, 1471–1474; Angew. Chem. Int. Ed.* **2011**, 50, 1435–1438; *Angew. Chem. Int. Ed.* **2011**, *50*, 1435–1438; b) M. Scheer, A. Schindler, J. Bai, B. P. Johnson, R. Merkle, R. Winter, A. V. Virovets, E. V. Peresypkina, V. A. Blatov, M. Sierka, H. Eckert, *Chem. Eur. J.* **2010**, *16*, 2092; c) M. Scheer, A. Schindler, C. Gröger, A. V. Viro-

vets, E. V. Peresypkina, *Angew. Chem.* **2009**, *121*, 5148; d) M. Scheer, A. Schindler, R. Merkle, B. P. Johnson, M. Linseis, R. Winter, C. E. Anson, A. V. Virovets, *J. Am. Chem. Soc.* **2007**, *129*, 13386; e) B. P. Johnson, F. Dielmann, G. Balázs, M. Sierka, M. Scheer, *Angew. Chem.* **2006**, *118*, 2533; *Angew. Chem. Int. Ed.* **2006**, *45*, 2473; f) M. Scheer, J. Bai, B. P. Johnson, R. Merkle, A. V. Virovets, C. E. Anson, *Eur. J. Inorg. Chem.* **2005**, 4023; g) J. Bai, A. V. Virovets, M. Scheer, *Science* **2003**, *300*, 781.

[8] K. D. M. Harris, E. Y. Cheung, *Chem. Soc. Rev.* **2004**, *33*, 526.

[9] R. Blom, T Brück, O. J. Scherer, *Acta Chem. Scand.* **1989**, *43*, 458.

[10] See the Supporting Information.

[11] J. C. C. Chan, G. Brunklaus, *Chem. Phys. Lett.* **2001**, *349*, 104.

[12] D. Massiot, F. Fayon, M. Capron, I. King, S. Le Calvé, B. Alonso, J-O. Durand, B. Bujoli, Z. Gan, G. Hoatson, *Magn. Reson. Chem.* **2002**, *40*, 70.

[13] M. Detzel, G. Friedrich, O. J. Scherer, G. Wolmershäuser, *Angew. Chem.* **1995**, *107*, 1454; *Angew. Chem. Int. Ed. Engl.* **1995**, *34*, 1321.

[14] a) M. Carravetta, M. Edén, X. Zhao, A. Brinkmann, M. H. Levitt, *Chem. Phys. Lett.* **2000**, *321*, 205; b) A. Brinkmann, M. H. Levitt, *J. Chem. Phys.* **2001**, *115*, 357.

[15] *CrysAlis RED*, *ABSPACK*, Oxford Diffraction Ltd., *SADABS*, Bruker AXS Inc.

[16] A. Altomare, M. C. Burla, M. Camalli, G. L. Cascarano, C. Giacovazzo, A. Guagliardi, A. G. G. Moliterni, G. Polidori, R. Spagna, *J. Appl. Crystallogr.* **1999**, *32*, 115–119.

[17] G. M. Sheldrick, *Acta Crystallogr. Sect. A* **2008**, *64*, 112–122.

Received: July 8, 2011
Published online: December 23, 2011

